Preconditions and limitations of the postulate of scalar-dissipation–conductivity independence in a variable conductivity medium

Gaurav Kumar, Sharath S. Girimaji,* and Johannes Kerimo
Department of Aerospace Engineering, Texas A&M University, College Station, Texas 77843-3141, USA
(Received 10 August 2010; revised manuscript received 25 April 2011; published 21 October 2011)

Classical turbulent mixing paradigm—ingrained in scaling laws and closure models—is revisited in a variable-conductivity inhomogeneous medium. We perform direct numerical simulations to study the evolution of a passive scalar (temperature) field in a fluid with large conductivity gradients and investigate the behavior of scalar dissipation, conditional scalar dissipation, and velocity-to-scalar time scale ratio. Subject to the conditions of the investigation, it is found that these mixing characteristics become reasonably insensitive to conductivity after about one-third eddy turnover time. While the results support the classical paradigm, important preconditions and limitations are clearly identified.

DOI: 10.1103/PhysRevE.84.046318 PACS number(s): 47.51.+a, 47.27.ek, 47.27.tb

I. INTRODUCTION

Scalar mixing in inhomogeneous media is of importance in many fields of current interest including energy, environment, and manufacturing. Specific examples include chemical processing and synthesis, pollutant dispersion in oceans and atmosphere, and combustion in power plants and engines. In many of these cases, scalar mixing is the rate controlling process that critically determines the outcome. Scalar mixing statistics of general importance are variance, dissipation, conditional dissipation, and velocity-to-scalar time scale ratio. Variance ($\langle\phi^2\rangle$) is a measure of the degree of unmixedness of the scalar. Scalar dissipation (ε_s) is the rate at which the variance is dissipated and hence is the most direct measure of the rate of mixing. Also important is the relation between time scales of the scalar field (τ_ϕ) and velocity field (τ_u). Conditional scalar dissipation is important as it determines the rate of evolution of the probability density function of the scalar field.

A. Classical mixing paradigm

Turbulent scalar mixing has been well studied in literature over the past few decades [1–7]. With the advent of large-scale computations, further inquiries, not possible with experimental investigations, have been made [8–12]. The studies indicate an intricate process in which turbulent fluctuations advect the scalar field over a wide range of flow scales leading to increased mixing rates. While many details of the mixing process vary based on specific flow features or prevailing nondimensional parameters, several common characteristics can be easily identified. The inferences lead to the following classical turbulent mixing paradigm.

(1) In an unmixed scalar field, scalar fluctuations are initiated at large scales of motion by the stirring action of the turbulent velocity field.

(2) The fluctuations then cascade down to smaller scales of motion where they are dissipated (completely mixed) by molecular action.

(3) The scalar cascade rate is determined by the variance and scalar time scale: cascade rate $\sim \langle\phi^2\rangle/\tau_\phi$. As passive scalar fluctuations are neither created nor destroyed in the intermediate scales, the scalar dissipation rate must equal the scalar cascade rate under equilibrium conditions: $\varepsilon_s \equiv \langle\kappa\frac{\partial\phi}{\partial x_i}\frac{\partial\phi}{\partial x_i}\rangle \sim \frac{\langle\phi^2\rangle}{\tau_\phi}$, where κ is conductivity and τ_ϕ is the characteristic scalar time scale as mentioned before. Throughout the paper, the symbol $\langle\cdot\rangle$ is used to represent spatial averaging. The cascade and scalar dissipation rate are strongly influenced by the initial length scales of velocity and scalar fields [5,8,13].

(4) Invoking the scalar analog of Taylor's viscosity-dissipation postulate [14,15], it is inferred that scalar dissipation is independent of conductivity or diffusivity as appropriate [12]. The value of conductivity (scalar diffusivity) determines only the extent of inertial scales or equivalently the steepness of the scalar gradient. The magnitude of the scalar gradient adjusts itself to the local conductivity, leading to scalar dissipation becoming equal to the scalar variance cascade rate.

(5) Since the scalar field is advected by the velocity field, the scalar time scale is proportional to that of the velocity field under equilibrium cascade conditions: $\tau_\phi \sim \tau_u \equiv \frac{k}{\varepsilon}$, where k is turbulent kinetic energy and ε is its dissipation rate. The proportionality constant in this scaling is also strongly dependent on the initial velocity-to-scalar length scale ratio [13].

(6) Finally, the conditional scalar dissipation is only a function of the scalar value and total scalar dissipation: $\langle\kappa\frac{\partial\phi}{\partial x_i}\frac{\partial\phi}{\partial x_i}|\phi=\theta\rangle = f(\varepsilon_\phi,\theta)$. Thus the conditional scalar dissipation is also insensitive to conductivity (diffusivity) [16].

This classical paradigm has been examined in a constant conductivity (diffusivity) medium by varying the large-scale fluctuations and length scale ($\frac{\langle\phi^2\rangle}{\tau_\phi}$) and many studies conclude that the scalar dissipation ($\varepsilon_s \equiv \langle\kappa\frac{\partial\phi}{\partial x_i}\frac{\partial\phi}{\partial x_i}\rangle$) adjusts accordingly. However, the postulate has not been investigated when the cascade rate is held spatially constant and conductivity (diffusivity) varies in time and space.

B. Mixing in inhomogeneous medium and research objective

Many applications involve scalar field mixing in heterogeneous mixtures characterized by steep spatiotemporal variations in transport properties. This evokes the following question: "can the classical paradigm be extended to inhomogeneous medium?" The validity in homogeneous medium hinges on the delicate balance between the large-scale spectral

*girimaji@aeromail.tamu.edu

cascade rate and dissipation, which occurs at small scales. In inhomogeneous media, such a balance may not be possible for several reasons. First, the rapid spatial and temporal changes in scalar conductivity may not allow sufficient time for scalar gradients to adapt to local transport properties. Secondly, spatial inhomogeneity in conductivity may give rise to new transport terms in the scalar dissipation evolution equation. Finally, any disparity between viscosity and conductivity could possibly cause the relationship between velocity and scalar time scales to become spatially variant. Thus motivated, the objective of this work is to revisit the classical paradigm in a turbulent medium with strong spatiotemporal variations in transport properties. Equally importantly, this work will provide further assessment of the classical postulates, but in a flow setup completely different from those considered in previous literature.

C. Velocity versus scalar field—similarities and differences

In a related prior work [15], we investigated the effect of steep viscosity variations on the dissipation-viscosity independence postulate [14], which forms the centerpiece of many widely used turbulence closure proposals. It was confirmed, subject to the conditions of the investigation, that dissipation was impervious to steep spatial gradients in viscosity. As suggested by Taylor, the square of the velocity gradients varies inversely with viscosity rendering the dissipation independent of viscosity. It is natural to expect such behavior from scalar fields as well. However, scalar field evolution, while similar to that of velocity field in many aspects, exhibits some notable differences. It was pointed out by Sreenivasan [6] that the small-scale isotropy and universality are less evident in scalar fields compared to velocity fields. Furthermore, it was pointed out that there are fundamental differences in the manner in which fluctuations cascade down to small scales. Warhaft [17] observes that a passive scalar governed by a linear equation displays characteristics very different from the advecting velocity field: while the velocity field is Gaussian, the probability density function of the scalar field has exponential tails. The scalar field exhibits strong inertial subrange intermittency even at low Reynolds number, a feature typically absent in velocity fields. Yeung [9] studied the Lagrangian statistical properties of velocity and passive scalar fields using direct numerical simulations (DNS) for the case of stationary isotropic turbulence with uniform mean scalar gradients. The findings confirm that scalar dissipation is highly intermittent and that it becomes decorrelated temporally more rapidly than energy dissipation. Donzis *et al.* [11] performed simulations of passive scalar mixing in high Reynolds number turbulence and found that small scales in scalar field retain the anisotropy of large scales even though a inertial-convective range is evident. Their data also suggests that the probability density functions of energy dissipation, enstrophy, and scalar dissipation may converge to the same shape at high enough Reynolds number. These differences between the velocity and scalar fields indicate that the velocity findings of [15] cannot be directly taken to be valid for scalar fields. Thus a full-fledged reexamination of the classical mixing paradigm for the inhomogeneous conductivity field is called for.

The remainder of the paper is arranged as follows. In Sec. II, the problem description is given along with the governing equations. The numerical method and cases studied are described in Sec. III. The results are presented and analyzed in Sec. IV. The paper concludes in Sec. V with a brief summary of the findings in the current work and identification of avenues for future investigations.

II. PROBLEM DESCRIPTION AND THEORY

Turbulent combustion involves complex interplay between fluid, thermodynamic, and chemical processes. Investigation of fundamental mixing mechanisms in such a complex flow field would render the problem intractable. Our approach is to devise a simple flow in which the effect of transport property variation can be considered in isolation without the complicating influence of other phenomena, such as chemical reaction, heat release, or variations in thermodynamic properties. Accordingly, we follow the line of investigation used by Lee *et al.* [15] to establish the effect of strong spatiotemporal viscosity gradients on dissipation of kinetic energy.

We consider incompressible decaying turbulence in a periodic computational box filled with a heterogeneous mixture of two species of equal density but vastly different transport properties. The mixture composition is indicated by mixture fraction—$f(\boldsymbol{x},t)$—which takes the value of zero in low conductivity (κ_l) species and unity in high conductivity ($\kappa_h = 5\kappa_l$) species. The two fluids are initially segregated, each occupying one half (along the x direction) of the box. A turbulent velocity field [$\boldsymbol{u}(\boldsymbol{x},t)$] and a passive scalar (temperature) field [$\phi(\boldsymbol{x},t)$] are resident in this heterogeneous medium. Throughout the paper, the term scalar will correspond to the temperature field and not that of species mixture fraction. The velocity and scalar fields are initially homogeneous, isotropic, and specified using standard schemes [18]. The initial length scale of the velocity and scalar fields are equal at about one-eighth of the computational box length. While the initial scalar gradient field is spatially homogeneous, scalar dissipation in the two halves of the box differs by a factor of 5 due to the difference in conductivities. With time, the turbulence field evolves chaotically, advecting the scalar field and the two species. Owing to the length and time scale disparities, the scalar field mixes much more rapidly than the two species. Under these conditions, the scalar field evolves in a medium with strong spatiotemporal variations of conductivity. This is the time duration of interest in this study. The transport properties of relevance are scalar conductivity (κ), fluid viscosity (μ), and diffusivity between the two species (D). The corresponding dimensionless parameters are the Schmidt number (viscosity/diffusivity), Reynolds number, and Prandtl number (viscosity/conductivity).

It must be pointed out at the very outset that, as in the preceding work [15], some of the details encountered in practical flows—density variations, heat release, and boundary effects—are not considered here. These complicating details are application-dependent and can possibly obscure the fundamental physical phenomena under investigation. The heat release effects manifest in our idealized problem through the initial transport property variations and their subsequent evolution. In the same spirit, some of the higher-order

mixing effects—the influence of initial velocity-scalar length scale ratio—will not be investigated in this work. For those discussions, the reader is referred to [13]. In this work, we will restrict ourselves to an initial length scale ratio of nearly unity and investigate only the influence of transport property variations.

The evolution of velocity field is governed by the mass (1) and momentum (2) conservation equations. The mixing process is governed by the mixture-fraction (3) and scalar (4) evolution equations:

$$\frac{\partial u_i}{\partial x_i} = 0, \tag{1}$$

$$\frac{\partial u_i}{\partial t} + \frac{\partial u_i u_j}{\partial x_j} = -\frac{\partial p}{\partial x_i} + \frac{\partial}{\partial x_j}\left(\mu(f)\frac{\partial u_i}{\partial x_j}\right), \tag{2}$$

$$\dot{f} \equiv \frac{\partial f}{\partial t} + \frac{\partial f u_j}{\partial x_j} = \frac{\partial}{\partial x_j}\left(D(f)\frac{\partial f}{\partial x_j}\right), \tag{3}$$

$$\frac{\partial \phi}{\partial t} + \frac{\partial u_j \phi}{\partial x_j} = \frac{\partial}{\partial x_j}\left(\kappa(f)\frac{\partial \phi}{\partial x_j}\right). \tag{4}$$

The transport properties (κ,μ,D) are functions of mixture fraction f and are calculated using mixture laws. Different mixture laws considered in the study are given in Eqs. (8) and (9).

To set the context for examining Taylor's postulate for scalars, the evolution equation for scalar dissipation $(\epsilon_s = \langle \kappa \frac{\partial \phi}{\partial x_j}\frac{\partial \phi}{\partial x_j}\rangle)$ for a variable conductivity (κ) mixture is shown:

$$\frac{\partial \epsilon_s}{\partial t} + \frac{\partial}{\partial x_k}\left\langle \kappa u_k \frac{\partial \phi}{\partial x_j}\frac{\partial \phi}{\partial x_j}\right\rangle = T - H + \left\langle \dot{\kappa}\frac{\partial \phi}{\partial x_j}\frac{\partial \phi}{\partial x_j}\right\rangle - 2\frac{\partial}{\partial x_j}\left\langle \kappa \frac{\partial \phi}{\partial x_j}\frac{\partial}{\partial x_k}\left(\kappa \frac{\partial \phi}{\partial x_k}\right)\right\rangle. \tag{5}$$

The terms $H[= 2\langle \frac{\partial}{\partial x_j}(\kappa \frac{\partial \phi}{\partial x_j})\frac{\partial}{\partial x_k}(\kappa \frac{\partial \phi}{\partial x_k})\rangle]$ and $T(= -2\langle \kappa \frac{\partial u_k}{\partial x_j}\frac{\partial \phi}{\partial x_k}\frac{\partial \phi}{\partial x_j}\rangle)$ represent destruction and generation of scalar dissipation, respectively. The third term on the right-hand side (RHS) accounts for the spatiotemporal variation of conductivity ($\dot{\kappa}$ denotes substantial derivative) and is present only in heterogeneous mixtures. Finally, the fourth term on the RHS represents the transport effects. A detailed discussion of these terms in the context of mechanical dissipation is given in [15]. The scalar analog is as follows: conductivity is present in every term on the RHS of the scalar dissipation equation (5) and hence appears to have a major role. Let us consider each term individually. The transport term (fourth term on the RHS) involves the gradient of a statistic and hence can be taken to be negligible in comparison with other terms. In a homogeneous medium, the third term on the RHS is absent.

According to the classical scaling arguments [7], both generation and destruction terms are individually dependent on diffusivity, but their difference is independent of diffusivity, rendering Taylor's postulate valid. The validity of Taylor's postulate in a heterogeneous medium hinges on (i) the balance between T and H being maintained and (ii) the third term on the RHS being much smaller than the difference between T and H. It is evident that dominance of the third term can completely change the mixing physics and render it completely dependent on diffusivity variation. Therefore, the length scale of κ variation critically determines the extent of applicability of the classical paradigm to a variable transport-property medium.

In this work, we will examine the conductivity-scalar dissipation relation in an inhomogeneous medium wherein viscosity-dissipation independence has been satisfactorily established [15]. It must be mentioned at the very outset that the viscosity-dissipation independence does not guarantee a similar outcome for the scalar field. As pointed out earlier, the scalar fields exhibit inertial range intermittency even at low Reynolds numbers [17] and that can be expected to play a role in the present study.

III. NUMERICAL APPROACH AND SIMULATION PARAMETERS

Direct numerical simulation (DNS) of decaying turbulence is performed in a cubic domain with 256^3 grid points ($N_x = N_y = N_z = 256$). The gas kinetic scheme, developed in [19] and validated for DNS of turbulence in [18] and [15], is used for computations. Although kinetic-theory–based DNS computational methods are relatively new, many recent works have established the accuracy and utility of such approaches [20–23]. Periodic boundary conditions are employed in all directions. Simulations start from a statistically homogeneous, isotropic, and divergence-free velocity field with the initial energy spectrum (in Fourier space $\boldsymbol{k}$) given by

$$E(k,0) = \frac{\hat{u}_i \hat{u}_i^*}{4\pi k^2} = Ak^4 e^{-Bk^2}, \quad k = \sqrt{k_x^2 + k_y^2 + k_z^2}. \tag{6}$$

Initially, only a narrow band of wave numbers are energized: $k \in [1,8]$. The steps involved in generating an initial velocity field are as follows.

(1) Generate an initial velocity field (u,v,w) in the physical space ($N_x \times N_y \times N_z$ points) using a "uniform random number generator" with individual velocity components in the range $(-1, +1)$.

(2) Transform the velocity field to Fourier space using forward discrete Fourier transform.

(3) Impose the incompressibility condition $(\vec{\hat{u}} \cdot \vec{k} = 0)$ by projecting $\vec{\hat{u}}$ on the plane normal to $\vec{k}$: $\vec{\hat{u}}^I = \vec{\hat{u}} - \vec{k}(\vec{k} \cdot \vec{\hat{u}})/k^2$. Replace $\vec{\hat{u}}$ with $\vec{\hat{u}}^I$: $\vec{\hat{u}} \rightarrow \vec{\hat{u}}^I$.

(4) Impose the required energy spectra condition $E(k,0) = Ak^4 e^{-Bk^2}$ and wave number restriction:

$$\vec{\hat{u}} \rightarrow \frac{\vec{\hat{u}}}{|\vec{\hat{u}}|}\sqrt{\frac{E(k,0)}{4\pi k^2}} \quad \text{if} \quad k \in [1,8], \quad \text{else} \quad \vec{\hat{u}} = 0. \tag{7}$$

(5) Transform back to physical space using inverse discrete Fourier transform.

Such a scheme yields a random, isotropic, and incompressible velocity field satisfying the desired energy spectra. A similar procedure (except step 3) is followed for the initial scalar field generation.

All simulations employ the same initial and boundary conditions for the velocity and scalar fields. Since the objective

TABLE I. Simulation cases A–E: Taylor microscale Reynolds number (Re_λ), Prandtl number (Pr), and Schmidt number (Sc) for left and right halves of the computational domain at time $t' = 0$. The mixing law used in each case is also shown ("uniform"means premixed).

Parameters		Cases				
		A	B	C	D	E
Re_λ	Left	64.49	64.49	64.49	64.49	193.47
	Right	64.49	64.49	64.49	64.49	38.69
Pr	Left	1.0	3.0	3.0	3.0	1.0
	Right	1.0	0.6	0.6	0.6	1.0
Sc	Left	1.0	1.0	1.0	1/4	3.0
	Right	1.0	1.0	1.0	5/3	0.6
Mixing law		Uniform	Linear	Wilkes	Wilkes	Wilkes

of this study is to examine the influence of transport properties, we perform five simulations with different combinations of initial Taylor microscale Reynolds number (Re_λ), Prandtl (Pr), and Schmidt (Sc) numbers as given in Table I. We also perform a baseline simulation in which all transport properties are spatially uniform. The initial condition for the nonpremixed heterogeneous simulations are such that the low conductivity species occupies the left half (along x) of the computational domain [$n_x = (1\text{–}128), f = 0, \kappa = \kappa_l$] and the high conductivity species occupies the other (right) half [$n_x = (128\text{–}256), f = 1, \kappa = \kappa_h = 5\kappa_l$].

We use two vastly different mixing laws, linear and Wilkes, for studying their effect on the validity of the classical paradigm. The linear mixture law is given by

$$\kappa(f) = f\kappa_h + (1-f)\kappa_l, \tag{8}$$

and the Wilkes mixture formula is given by

$$\kappa(f) = \frac{\kappa_h f}{f + (1-f)\Delta} + \frac{\kappa_l (1-f)}{(1-f) + \frac{\kappa_l}{\kappa_h} f\Delta}, \tag{9}$$

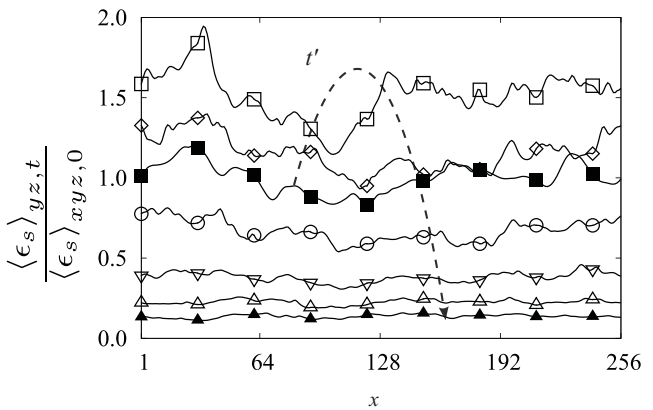

FIG. 1. Evolution of planar scalar dissipation $\langle \epsilon_s \rangle_{yz}$ for a single species case (case A). (■ : $t' = 0.0$; □ : $t' = 0.09$; ◇ : $t' = 0.18$; ○ : $t' = 0.27$; ▽ : $t' = 0.36$; △ : $t' = 0.45$; ▲ : $t' = 0.54$).

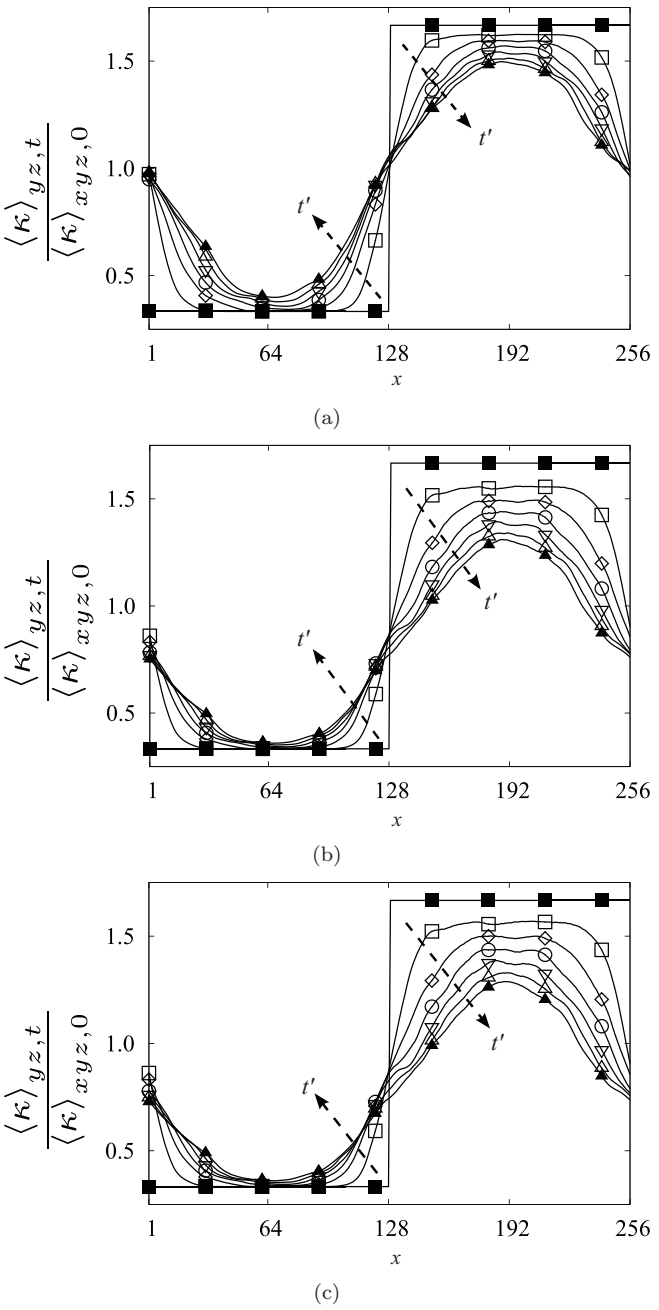

FIG. 2. Evolution of yz-plane-averaged conductivity $\langle \kappa \rangle_{yz}$ for a two species case: (a) case B; (b) case C; (c) case D (■ : $t' = 0.0$; □ : $t' = 0.09$; ◇ : $t' = 0.18$; ○ : $t' = 0.27$; ▽ : $t' = 0.36$; △ : $t' = 0.45$; ▲ : $t' = 0.54$).

where

$$\Delta = \frac{1}{4}\left[1 + \left(\frac{\kappa_h}{\kappa_l}\right)^{\frac{1}{2}}\right]^2.$$

In simulations with variable viscosity μ (or diffusivity D), the mixture law used for μ (or D) is the same as that used for conductivity κ.

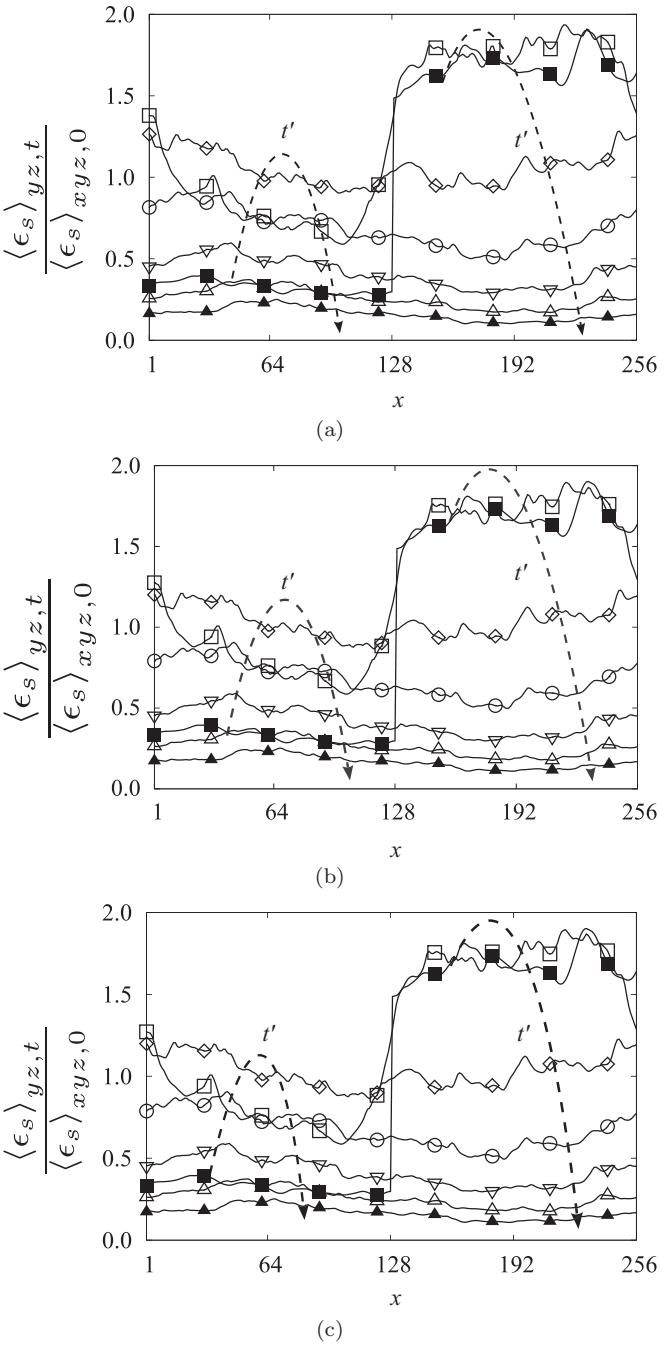

FIG. 3. Evolution of planar scalar dissipation $\langle \epsilon_s \rangle_{yz}$ for a two species case: (a) case B; (b) case C; (c) case D ($\blacksquare : t' = 0.0; \square : t' = 0.09; \diamond : t' = 0.18; \circ : t' = 0.27; \triangledown : t' = 0.36; \triangle : t' = 0.45; \blacktriangle : t' = 0.54$).

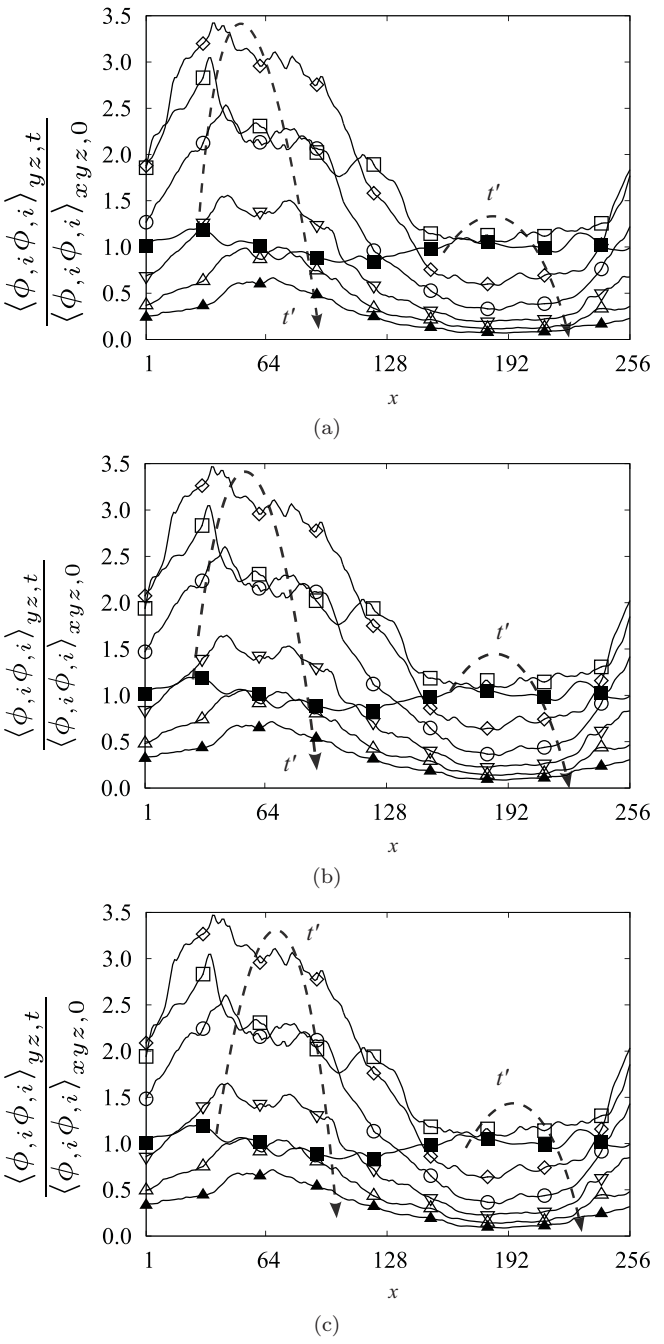

FIG. 4. Evolution of planar scalar gradient $\langle \phi_{,i}\phi_{,i} \rangle_{yz}$ for a two species case: (a) case B; (b) case C; (c) case D ($\blacksquare : t' = 0.0; \square : t' = 0.09; \diamond : t' = 0.18; \circ : t' = 0.27; \triangledown : t' = 0.36; \triangle : t' = 0.45; \blacktriangle : t' = 0.54$).

IV. RESULTS AND ANALYSIS

As turbulence evolves, the two species and the scalar field mix due to advection and diffusion. The species segregation makes the problem inhomogeneous along the x direction but homogeneity in preserved in the yz plane. Each yz plane corresponds to a different mixture composition. Hence the yz-plane-averaged statistics $\langle \cdot \rangle_{yz}$ are studied as a function of the x coordinate, at various stages of flow evolution. The initial eddy turnover time scale is used to nondimensionalize time as $t' = \epsilon_{s0} t / k_{s0}$. Plane-averaged quantities are nondimensionalized using volume average of the corresponding quantity at the initial time $\langle \cdot \rangle_{xyz,0}$ or at same time instant as appropriate.

First, we present the evolution of planar scalar dissipation for the baseline simulation—case A, where the two species are premixed. The conductivity is uniform throughout the box and is chosen to be $\kappa = (\kappa_l + \kappa_h)/2$, which is the average of the low and high conductivities used in simulations B–E. In Fig. 1, nondimensionalized plane-averaged scalar dissipation $\epsilon_s(x)$ has been presented for various stages of flow evolution. Due to the initial homogeneous and isotropic distribution of

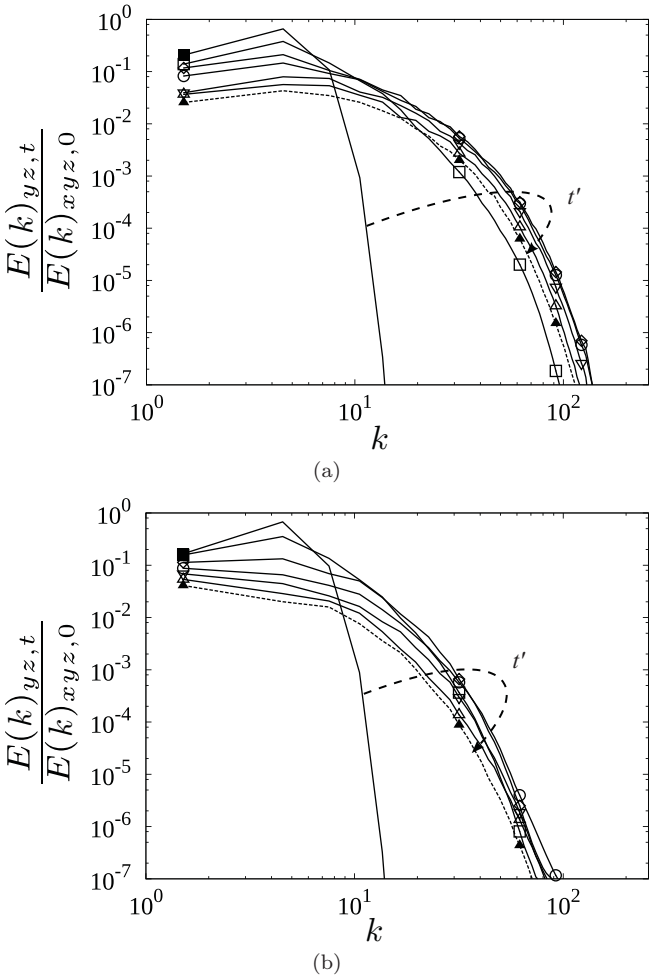

FIG. 5. Evolution of planar spectra in case C (two species case): (a) low conductivity plane $n_x = 64$; (b) high conductivity plane $n_x = 192$ ($\blacksquare : t' = 0.0; \square : t' = 0.09; \diamond : t' = 0.18; \circ : t' = 0.27; \triangledown : t' = 0.36; \triangle : t' = 0.45; \blacktriangle : t' = 0.54$).

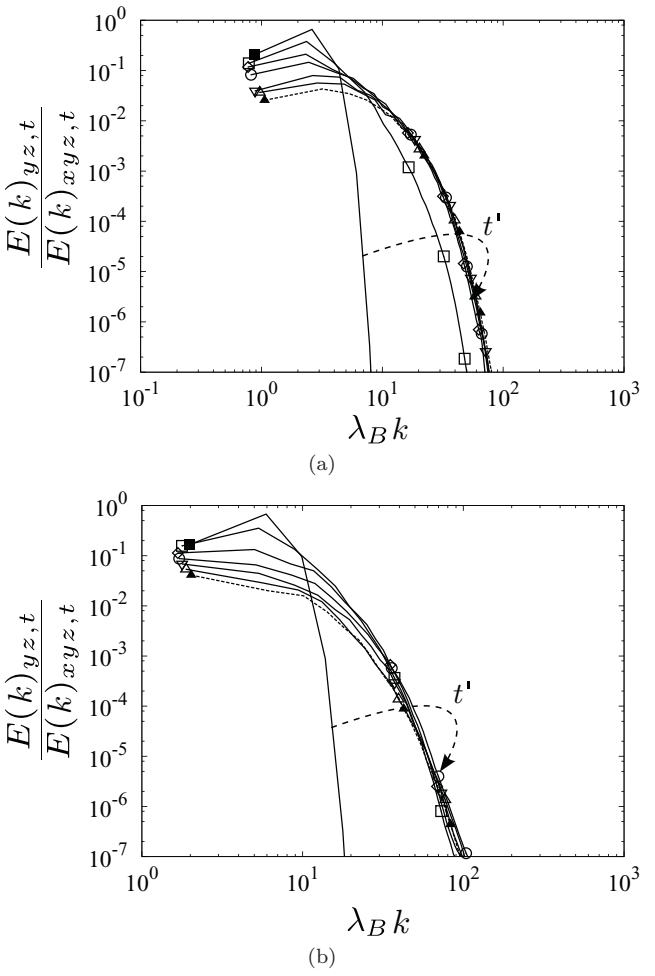

FIG. 6. Evolution of planar spectra in case C with wave numbers normalized with the Batchelor scale: (a) low conductivity plane $n_x = 64$; (b) high conductivity plane $n_x = 192$ ($\blacksquare : t' = 0.0; \square : t' = 0.09; \diamond : t' = 0.18; \circ : t' = 0.27; \triangledown : t' = 0.36; \triangle : t' = 0.45; \blacktriangle : t' = 0.54$).

the scalar ϕ and a spatially uniform κ, scalar dissipation is statistically uniform across the box. Scalar dissipation initially increases throughout the box and peaks at about $1/10$ eddy turnover time and decreases monotonically thereafter. An initial increase in the scalar dissipation is attributed to a nonlinear cascade, which generates smaller structures and steepens the scalar gradient. Subsequently, molecular action dissipates the small-scale structures resulting in weaker scalar gradients and reduced dissipation.

Next, we turn our attention to mixing in a heterogeneous medium. Our objective is to establish mixing characteristics of the scalar field during a time period when the mixture is still significantly heterogeneous. All simulations of heterogeneous cases yield similar results, so we only present results from cases B–D for the sake of brevity. The nondimensionalized yz-plane averaged conductivity variation along the x direction, $\langle\kappa\rangle_{yz}/\langle\kappa\rangle_{xyz,0}$, is plotted in Fig. 2 at various times ($t' < 0.6$) for cases B, C, and D. Initially, the conductivity is five times larger on one side than the other. After about one-half eddy turnover time, the two species mix to a reasonable extent, but still the ratio of maximum to minimum conductivity is about 4 in all cases (B–E).

The evolution of scalar dissipation for cases B, C, and D is shown in Figs. 3(a), 3(b), and 3(c), respectively. Initially, the scalar dissipation is five times larger on the high conductivity side. Then, as mixing proceeds, scalar dissipation increases throughout the domain due to cascade. The cascade process generates smaller scales, and hence steepens the scalar gradient. The increase in scalar dissipation is higher in the low conductivity region compared to that in the high conductivity region. The peak of scalar dissipation is observed at around $1/5$ and $1/10$ eddy turnover time in low and high conductivity regions, respectively. Subsequently, scalar dissipation decays on both sides with the rate of decay being higher in the larger conductivity region. This differential decay works to reduce the disparity in scalar dissipation between the left and right halves of the domain. Toward the end of the simulation, scalar dissipation becomes more uniform along x than at earlier times. Scalar dissipation does not exhibit the strong dependence on x displayed by the conductivity at the corresponding time. Also, a comparison of the evolution of scalar dissipation in case B against that in cases C, D, and E shows the mixture law does not seem to affect the

final outcome—a relatively uniform distribution of the scalar dissipation. Importantly, at this time, yz-plane averaged scalar dissipation distribution in cases B–E becomes comparable to the corresponding distribution for case A. Thus the scalar dissipation is nearly uniform (i) in different regions of vastly different conductivity within one simulation and (ii) across all heterogeneous and homogeneous conductivity simulations. It must be mentioned that the "conductivity–scalar dissipation independence"is not as unequivocal as "viscosity-dissipation independence" demonstrated in [15]. Nevertheless, the dependence of scalar dissipation on conductivity is weak enough to endorse the scalar equivalent of Taylor's postulate in heterogeneous mixtures.

Despite a large difference in conductivity between the left and right halves, scalar dissipation is almost uniform because of the compensatory behavior of the scalar gradient. To demonstrate this, we show the evolution of the yz-plane averaged scalar gradient $\langle \phi_{,i}\phi_{,i}\rangle_{yz}$ for cases B, C, and D in Figs. 4(a), 4(b), and 4(c), respectively. The initial homogeneous and isotropic distribution of the scalar ϕ renders the initial distribution of the scalar gradient $\langle \phi_{,i}\phi_{,i}\rangle_{yz}$ to be uniform along x. However, as flow evolves, scalar gradient $\langle \phi_{,i}\phi_{,i}\rangle_{yz}$ grows more rapidly in the low conductivity region compared to the region of high conductivity. Thus, a high $\langle \phi_{,i}\phi_{,i}\rangle_{yz}$ in low $\langle \kappa\rangle_{yz}$ region and low $\langle \phi_{,i}\phi_{,i}\rangle_{yz}$ in high $\langle \kappa\rangle_{yz}$ region allows for a nearly uniform distribution of $\langle \kappa\phi_{,i}\phi_{,i}\rangle_{yz}$.

The planar scalar spectra for yz planes at $n_x = 64$ and $n_x = 192$ for case C are shown in Figs. 5(a) and 5(b), respectively. The broader planar scalar spectrum for the yz plane at $n_x = 64$ [Fig. 5(a)] compared to that at $n_x = 192$ [Fig. 5(b)] indicates the presence of smaller scales and hence steeper gradients in the low conductivity region. The low and high conductivity region planar spectra are also presented in Fig. 6, except with wave numbers normalized with the Batchelor scale:

$$\lambda_B = \left(\frac{\nu\kappa^2}{\epsilon}\right)^{\frac{1}{4}}. \tag{10}$$

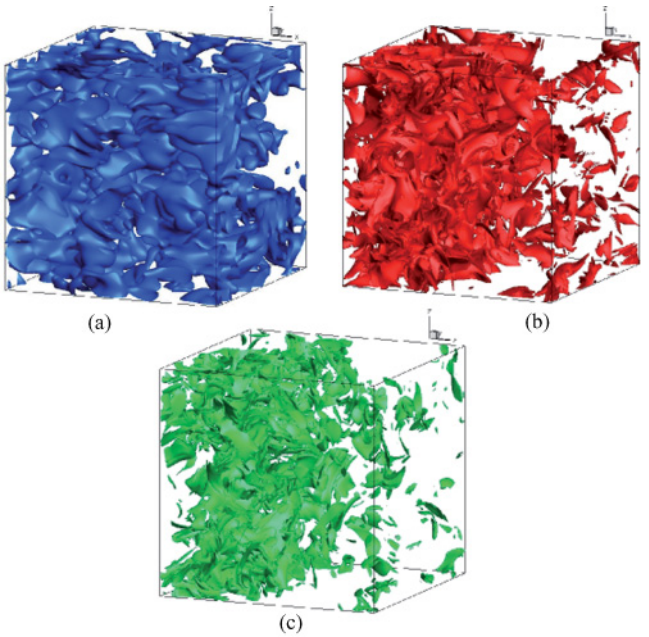

FIG. 7. (Color online) Isosurfaces of scalar gradient $(\phi_{,i}\phi_{,i})$ for a two species case (case C): (a) time $t' = 0.00$; (b) time $t' = 0.36$; (c) time $t' = 0.54$.

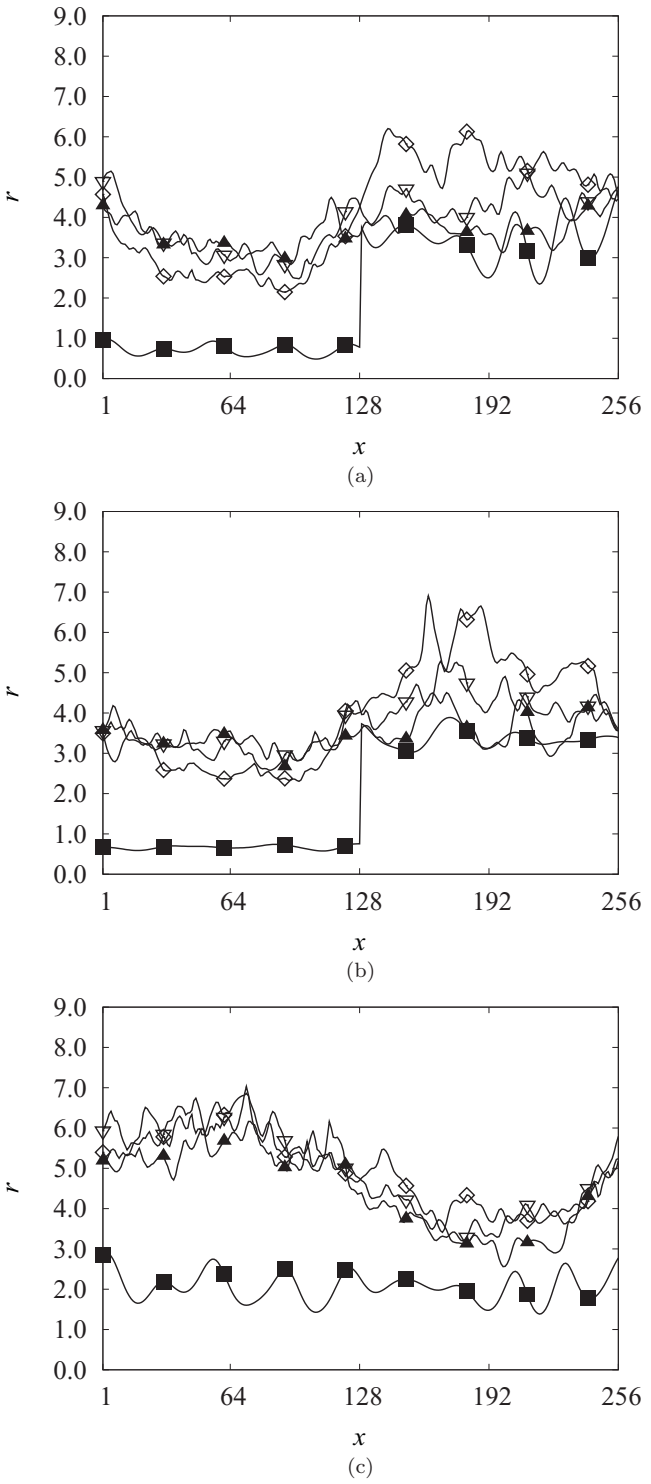

FIG. 8. Evolution of velocity-to-scalar time scale ratio r with time t': (a) case B; (b) case C; (c) case E (■ : $t' = 0.0$; ◇ : $t' = 0.18$; ▽ : $t' = 0.36$; ▲ : $t' = 0.54$).

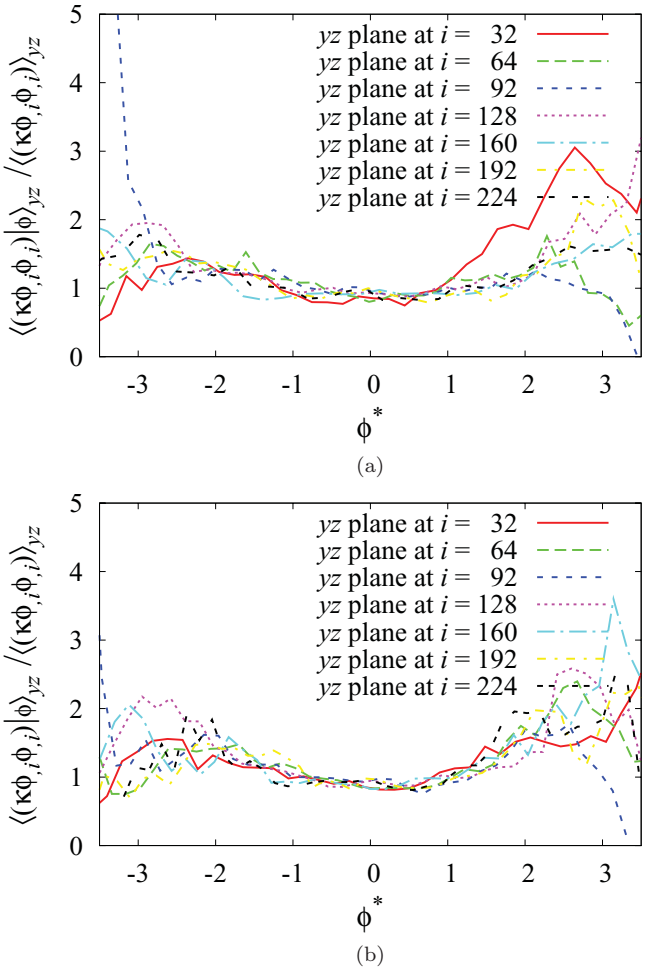

FIG. 9. (Color online) Conditional scalar dissipation for different yz planes for case C: (a) time $t' = 0.45$; (b) time $t' = 0.54$.

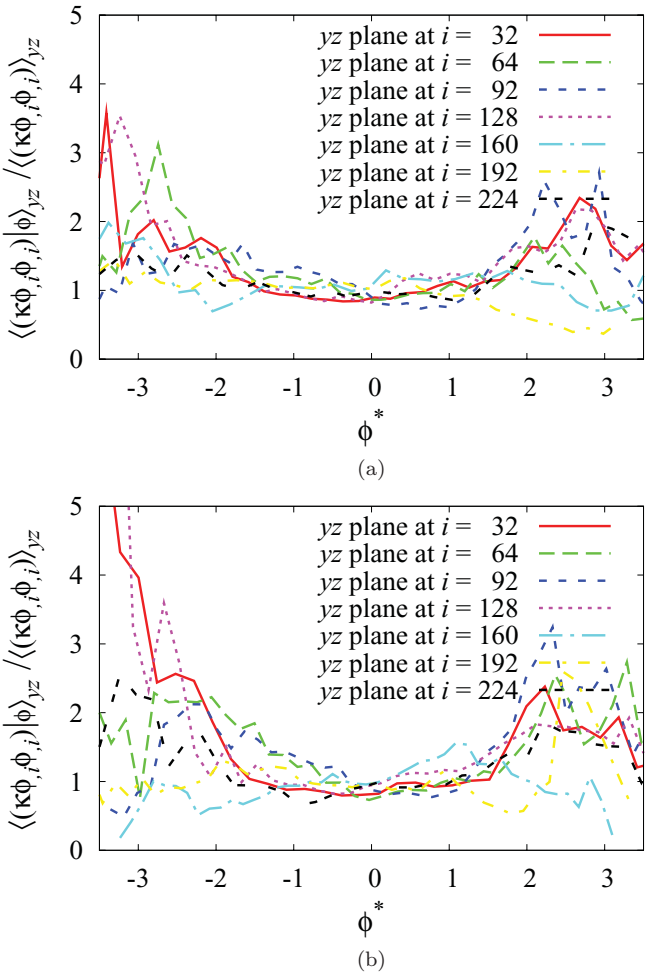

FIG. 10. (Color online) Conditional scalar dissipation for different yz planes for case E: (a) time $t' = 0.45$; (b) time $t' = 0.54$.

The normalized spectra show collapse at later stages of mixing. The dependence of the normalized spectrum on the Prandtl number is of interest and will be investigated in a separate study.

To visualize the difference in scales of motion present in the two halves of the box, isosurfaces of scalar gradient magnitude ($\phi_{,i}\phi_{,i}$) are presented for simulation case C at three different stages of flow evolution in Fig. 7. Initially, the isosurfaces are smooth and uniformly distributed throughout the computational domain as seen in Fig. 7(a). From Figs. 7(b) and 7(c), we observe that, as flow evolves, isosurfaces become more wrinkled on the lower conductivity side, thus indicating the presence of smaller scales. In contrast, the right half of the box (higher κ) is devoid of small scales. However, despite this difference in length scales of the scalar field in the two halves of the box at later times, the scalar dissipation is nearly identical. The results from Figs. 4, 5, and 7 clearly confirm that small scales in the scalar field adapt to the imposed conductivity variation limiting the dependence of the scalar dissipation rate on conductivity.

An important "scalar mixing modeling"assumption is that the mixing time scale is proportional to that of the velocity field. To verify this scaling in a heterogeneous mixture, we investigate the behavior of velocity-to-scalar time scale ratio r,

$$r \equiv \frac{\tau_u}{\tau_\phi} = \frac{\langle 3u^2\rangle/\langle\epsilon\rangle}{\langle\phi^2\rangle/\langle\epsilon_s\rangle}. \tag{11}$$

The velocity-to-scalar time scale ratio for two species cases B, C, and E are shown in Figs. 8(a), 8(b), and 8(c), respectively. The results show that the time scale ratio is nearly independent of the Prandtl number, but a weak function of the Reynolds number. Overall, the value of velocity-to-scalar time scale ratio r computed in the present work is well within the range reported in [12], in which the time scale results are compiled from a variety of experiments and numerical simulations. As mentioned in the Introduction, we do not address the effect of the initial length scale ratio in this work.

The evolution of conditional scalar dissipation $\langle\kappa\frac{\partial\phi}{\partial x_i}\frac{\partial\phi}{\partial x_i}|\phi\rangle_{yz}/\langle\kappa\frac{\partial\phi}{\partial x_i}\frac{\partial\phi}{\partial x_i}\rangle_{yz}$ is investigated next. Results from different yz planes for cases C and E are presented in Figs. 9 and 10, respectively, at eddy-turnover times $t' = 0.45$ and 0.54. The conditional scalar dissipation is shown as a function of normalized scalar value: $\phi^* = [\phi - \langle\phi\rangle(t)]/\langle\phi'^2(t)\rangle$. As turbulence evolves and scalars mix, conditional scalar dissipation from planes of different conductivity $\langle\kappa\rangle_{yz}$ values become nearly

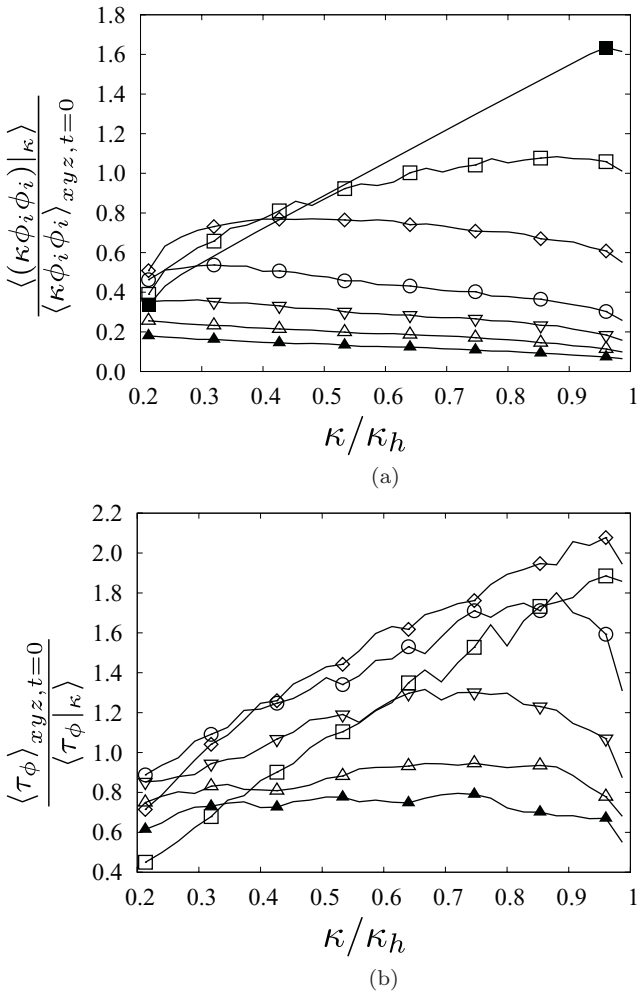

FIG. 11. Case B: (a) evolution of mean scalar dissipation conditioned on κ normalized by volume averaged scalar dissipation at time $t' = 0$; (b) scalar frequency conditioned on κ normalized by volume averaged value at time $t' = 0$ ($\blacksquare : t' = 0.0; \square : t' = 0.09; \diamond : t' = 0.18; \circ : t' = 0.27; \triangledown : t' = 0.36; \triangle : t' = 0.45; \blacktriangle : t' = 0.54$).

indistinguishable. Moreover, the normalized conditional scalar dissipation is nearly unity in the interval $\phi^* = (-2,2)$, indicating a nearly Gaussian distribution. However, outside of the range $\phi^* = (-2,2)$, the conditional scalar dissipation is much higher. This may be evidence of the scalar intermittency mentioned in the Introduction. Interestingly, the conditional scalar dissipation for all x planes exhibits the same qualitative behavior, indicating that the intermittency features are not strongly dependent on the conductivity values. Based on these results and similar ones from other simulations, we conclude that conditional scalar dissipation (including intermittency characteristics) is reasonably impervious to conductivity, viscosity, or species diffusivity (D).

The dependence of various scalar statistics on diffusivity was examined thus far in terms of yz-plane-averaged statistics. The mean value of diffusivity (conductivity) on each yz plane varies strongly in the x direction as demonstrated in Fig. 2. Due to the stochastic nature of turbulence, diffusivity values also fluctuate moderately on each plane about the mean value. A more precise assessment of the dependence on diffusivity can be obtained by conditioning the statistics on a fixed diffusivity value rather than on an x coordinate. The evolution of mean scalar dissipation and scalar frequency (dissipation/variance) conditioned on diffusivity values is presented in Figs. 11(a) and 11(b), respectively, for the simulation case B. Scalar dissipation is initially strongly dependent on diffusivity. Very rapidly, the scalar dissipation becomes nearly insensitive to diffusivity. During later times, the higher diffusivity locations surprisingly exhibit lower dissipation. This anomalous behavior can be attributed to the fact that the fluctuations on the high diffusivity side are much lower at later times due to the larger dissipation at the early transient times. This disparity in scalar fluctuations can be accounted for by normalizing the diffusivity-conditioned dissipation with diffusivity-conditioned variance. The conditioned frequency $\langle f_\phi|\kappa\rangle = 1/\langle\tau_\phi|\kappa\rangle = \langle\epsilon_s|_\kappa\rangle/\langle(\phi-\bar{\phi})^2|_\kappa\rangle$ is plotted in Fig. 11(b). Initially, the conditioned frequency is a strong function of diffusivity. At early times, the frequency increases uniformly at all diffusivity values, as the scalar dissipation increases due to scalar fluctuations cascading down to smaller scales. After about one-third eddy turnover time, the frequency becomes nearly uniform everywhere. Figure 11 strongly supports the scalar equivalent of Taylor's postulate.

V. CONCLUSIONS

The objective of this work is to revisit the classical turbulent mixing paradigm for the case of inhomogeneous fluid media. Of specific interest is the dependence of scalar dissipation, conditional dissipation, and scalar-to-velocity ratio on transport properties. Previous validation studies in literature examine the validity of the postulate in a uniform-conductivity medium by varying the spectral cascade rate (large-scale fluctuation magnitude and length scale) and demonstrating that the dissipation changes accordingly. In contrast, here we maintain the cascade rate spatially uniform and vary the conductivity in space and time. Validity of the classical paradigm would entail that scalar dissipation be spatially uniform, despite strong variations in conductivity.

Toward this end, direct numerical simulations of scalar (temperature) mixing are performed in a flow field with steep variations in transport properties. The domain is a periodic cube and the resident turbulence is initially homogeneous and isotropic. The medium consists of two species of different transport properties, each of which initially occupies one-half of the computational domain. The fluctuating scalar field is initially homogeneous and has nearly the same length scale as the velocity field. Under these conditions, the scalar field can be regarded as mixing in a medium with strong spatiotemporal transport property gradients. The findings can be summarized as follows.

(1) It is found that fluctuating scalar gradients do adapt to the imposed conductivity variations rendering scalar dissipation nearly insensitive to conductivity. During the late stages of mixing, the yz-plane-averaged scalar dissipation is significantly more uniform along the x axis than yz-plane-averaged transport coefficients (conductivity, diffusivity, and viscosity), which exhibit up to 400% variation.

(2) The mean scalar frequency conditioned on a specific value of diffusivity is nearly independent of diffusivity.

(3) When appropriately normalized, conditional scalar dissipation also appears to be reasonably insensitive to conductivity. The extreme values of conditional scalar dissipation appear to exhibit intermittent behavior. However, the intermittency characteristics do not appear to depend on conductivity.

(4) Importantly, the scalar-to-velocity time scale ratio is also found to be reasonably insensitive to the Prandtl number, but weakly dependent on the Reynolds number.

The investigation identifies some important avenues for future investigations as follows.

(1) The diffusivity-scalar dissipation independence is not as conclusive as the viscosity-mechanical dissipation under similar conditions [15]. The role of the missing physical effect—pressure—must be clearly established.

(2) The scalar spectrum normalized by Batchelor scale is self-similar for a given Prandtl number. However, the self-similarity is restricted to small scales. The dependence of the self-similar shape on the Prandtl number deserves further examination.

(3) The apparent intermittent behavior of scalar gradients at extreme values is clearly of great interest. This also calls for a detailed investigation of intermittency, but first in the context of constant scalar diffusivity (conductivity).

Along with the results reported in the previous study [15], these findings reasonably support the applicability of Taylor's postulate in heterogeneous media. It must be emphasized that the findings are valid only for flows with initial scalar-to-velocity length scale ratio of order unity. If the scalar length scale is much smaller than that of the velocity field, additional effects may influence the results and consequently closure models must be used judiciously.

ACKNOWLEDGMENT

This work was supported by a NASA NRA Grant.

[1] G. I. Taylor, Proc. London Math. Soc. **20**, 196 (1921).
[2] S. Corrsin, J. Aeronaut. Sci. **18**, 417 (1951).
[3] K. R. Sreenivasan, S. Tavoularis, R. Henry, and S. Corrsin, J. Fluid Mech. **100**, 597 (1980).
[4] P. A. Durbin, Phys. Fluids **25**, 1328 (1982).
[5] Z. Warhaft and J. L. Lumley, J. Fluid Mech. **88**, 659 (1978).
[6] K. R. Sreenivasan, Proc. R. Soc. London Ser. A **434**, 165 (1991).
[7] P. S. Bernard and J. M. Wallace, *Turbulent Flow: Analysis, Measurement and Prediction* (Wiley, New York, 2002).
[8] V. Eswaran and S. B. Pope, Phys. Fluids **31**, 506 (1988).
[9] P. K. Yeung, J. Fluid Mech. **427**, 241 (2001).
[10] P. K. Yeung, D. A. Donzis, and K. R. Sreenivasan, Flow Turbulence Combust. **72**, 333 (2004).
[11] D. A. Donzis, P. K. Yeung, and K. R. Sreenivasan, Phys. Fluids **17**, 081703 (2005).
[12] D. A. Donzis, K. R. Sreenivasan, and P. K. Yeung, J. Fluid Mech. **532**, 199 (2005).
[13] J. R. Ristorcelli, Phys. Fluids **18**, 075101 (2006).
[14] G. I. Taylor, Proc. R. Soc. London Ser. A **151**, 421 (1935).
[15] K. Lee, S. S. Girimaji, and J. Kerimo, Phys. Rev. Lett. **101**, 074501 (2008).
[16] S. S. Girimaji, Phys. Fluids A **4**, 2529 (1992).
[17] Z. Warhaft, Annu. Rev. Fluid Mech. **32**, 203 (2000).
[18] J. Kerimo and S. S. Girimaji, J. Turbulence **8**, 1 (2007).
[19] K. Xu, J. Comput. Phys. **171**, 289 (2001).
[20] H. Yu, S. S. Girimaji, and L.-S. Luo, Phys. Rev. E **71**, 016708 (2005).
[21] H. Yu, S. S. Girimaji, and L.-S. Luo, J. Comput. Phys. **209**, 599 (2005).
[22] K. Lee, D. Yu, and S. S. Girimaji, Int. J. Comput. Fluid Dyn. **20**, 401 (2006).
[23] S. S. Girimaji, Phys. Rev. Lett. **99**, 034501 (2007).